

Out-of-plane high-temperature ferromagnetic monolayer CrSCl with large vertical piezoelectric response

San-Dong Guo¹, Xiao-Shu Guo¹, Yu-Tong Zhu¹ and Yee-Sin Ang²

¹*School of Electronic Engineering, Xi'an University of Posts and Telecommunications, Xi'an 710121, China*

²*Science, Mathematics and Technology (SMT), Singapore University of Technology and Design (SUTD), 8 Somapah Road, Singapore 487372, Singapore*

For two-dimensional (2D) material, piezoelectric ferromagnetism (PFM) with large out-of-plane piezoresponse is highly desirable for multifunctional ultrathin piezoelectric device application. Here, we predict that Janus monolayer CrSCl is an out-of-plane ferromagnetic (FM) semiconductor with large vertical piezoelectric response and high Curie temperature. The predicted out-of-plane piezoelectric strain coefficient d_{31} is -1.58 pm/V , which is higher than ones of most 2D materials (compare absolute values of d_{31}). The large out-of-plane piezoelectricity is robust against electronic correlation and biaxial strain, confirming reliability of large d_{31} . Calculated results show that tensile strain is conducive to high Curie temperature, large magnetic anisotropy energy (MAE) and large d_{31} . Finally, by comparing d_{31} of CrYX (Y=S; X=Cl, Br I) and CrYX (Y=O; X=F, Cl, Br), we conclude that the size of d_{31} is positively related to electronegativity difference of X and Y atoms. Such findings can provide valuable guidelines for designing 2D piezoelectric materials with large vertical piezoelectric response.

Keywords: Ferromagnetism, Piezoelectronics, 2D materials

Email:sandongyuwang@163.com

INTRODUCTION

The multifunctional 2D piezoelectric materials can give rise to unprecedented opportunities for intriguing physics, and provide a potential platform for multifunctional electronic devices[1]. The coexistence of piezoelectricity, electronic topology and ferromagnetism, namely piezoelectric quantum anomalous Hall insulator (PQAH), has been predicted in Janus monolayer Fe_2IX (X=Cl and Br)[2], which provides possibility to use the piezoelectric effect to control quantum anomalous Hall (QAH) effects. The piezoelectric properties of ferrovalley (FV) materials have been investigated[3, 4], and the anomalous valley Hall effect induced by piezoelectric effect has been proposed in GdCl_2 monolayer[4]. Searching for PFMs has been a research hotspot[5–10]. An eminent 2D PFM with a typical triangle lattice structure should meet these conditions: (1) the strong FM coupling, which means high Curie temperature; (2) the out-of-plane magnetic anisotropy, which means a long-range phase, not a quasi-long-range phase; (3) the large out-of-plane piezoresponse, which is highly desirable for ultrathin piezoelectric device application. However, the reported PFMs satisfy some of these conditions. For example NiCl_2 monolayer, the large out-of-plane piezoelectricity ($d_{31}=1.89 \text{ pm/V}$) has been predicted, but it has very weak FM coupling and in-plane magnetic anisotropy[10]. For InCrTe_3 monolayer, it has large FM coupling and out-of-plane magnetic anisotropy, but the out-of-plane piezoelectricity is weak ($d_{31}=0.39 \text{ pm/V}$)[9]. Therefore, searching for 2D PFMs with strong out-of-plane FM coupling and large vertical piezoelectric response is significant and challenging.

2D Janus materials have attracted increasing attention[11, 12], and the representative MoSSe

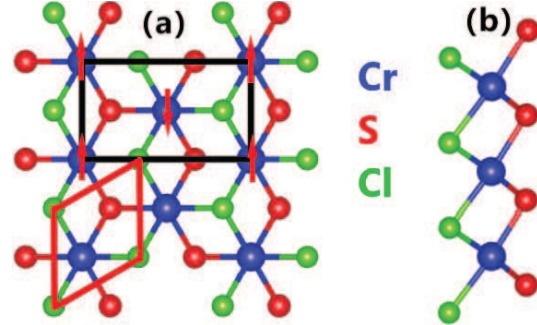


FIG. 1. (Color online) For Janus CrSCl monolayer, (a): top view and (b): side view of crystal structure. The primitive (rectangle supercell) cell is marked by red (black) lines. The red arrows represent the spin direction of Cr atoms.

monolayer has been successfully fabricated in experiment[13, 14]. Due to broken out-of-plane symmetry, the out-of-plane piezoelectricity can be observed in these Janus materials. Therefore, 2D Janus materials provide potential platform for searching good 2D PFMs. Recently, Janus monolayer Cr-based dichalcogenide halides CrYX (Y=S, Se, Te; X=Cl, Br, I) have been predicted by the first-principle calculations, and the CrSX (X=Cl, Br, I) are FM semiconductors[15]. The size of out-of-plane piezoelectric coefficient may have a positive relation with electronegativity difference of X and Y atoms for Janus MXY materials with M sandwiched between X and Y[16].

Due to large electronegativity difference of S and Cl atoms, in this work, we detailedly explore the magnetic, electronic and piezoelectric properties of CrSCl. It is found that CrSCl possesses an out-of-plane magnetization and high Curie temperature. The predicted d_{31}

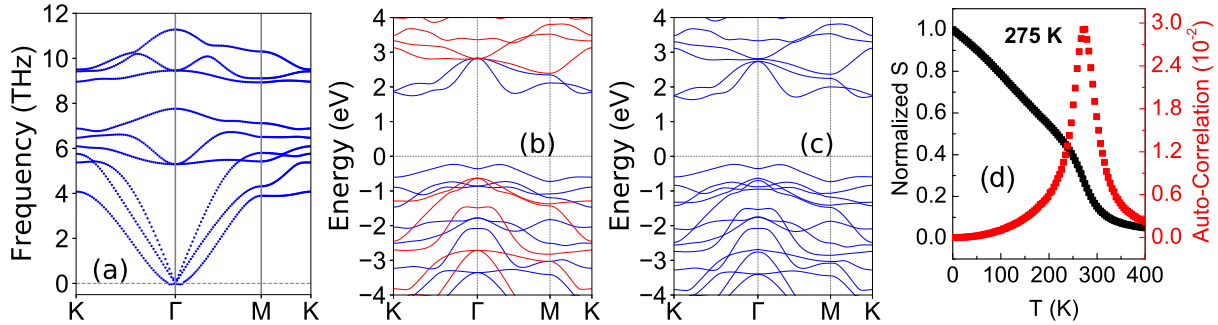


FIG. 2. (Color online) For Janus CrS_{Cl} monolayer, (a): the phonon dispersion curves; (b): the energy band structures with GGA; (c): the energy band structures with GGA+SOC; (d): the normalized magnetic moment (S) and auto-correlation as a function of temperature. In (b), the blue (red) lines represent the band structure in the spin-up (spin-down) direction.

is -1.58 pm/V , which is higher than ones (less than 1 pm/V) of most 2D materials (compare absolute values of d_{31}). More importantly, the large vertical piezoelectric response is robust against the electronic correlation and biaxial strain, which ensures high reliability of large d_{31} . Moreover, tensile strain can enhance FM coupling, out-of-plane MAE and d_{31} , which is in favour of eminent 2D PFM. Finally, we investigate d_{31} of CrYX (Y=S; X=Cl, Br, I) and CrYX (Y=O; X=F, Cl, Br), and the calculated results show that the large electronegativity difference of X and Y atoms indeed can give rise to large d_{31} .

COMPUTATIONAL DETAIL

Based on density functional theory (DFT)[17], the first-principle calculations are carried out by using the projector augmented wave (PAW) method as implemented in Vienna ab initio Simulation Package (VASP)[18–20]. The exchange-correlation functional is used by adopting generalized gradient approximation of Perdew, Burke and Ernzerhof (GGA-PBE)[21]. To consider on-site Coulomb correlation of Cr-3d electrons, we adopt $U=2.1 \text{ eV}$ [15] by the rotationally invariant approach proposed by Dudarev et al[22], where only the effective U (U_{eff}) based on the difference between the on-site Coulomb interaction parameter and exchange parameters is meaningful. The spin-orbital coupling (SOC) is included to calculate electronic structures and MAE of CrS_{Cl}. To attain reliable results, we set the energy cut-off of 500 eV, total energy convergence criterion of 10^{-8} eV and force convergence criteria of less than $0.0001 \text{ eV}\cdot\text{\AA}^{-1}$. We add a vacuum space of more than 16 \AA between slabs along the z direction to eliminate the spurious interactions. The phonon spectrum with a $5\times 5\times 1$ supercell is calculated by using the Phonopy code[23]. The Curie temperature is estimated by Monte Carlo (MC) simulations, as implemented in Mcsolver code[24]. A 40×40 supercell with periodic boundary conditions and 10^7 loops are used to perform the MC simulation using

Wolff algorithm. The elastic stiffness and piezoelectric stress tensors (C_{ij} and e_{ij}) are calculated by using strain-stress relationship (SSR) and density functional perturbation theory (DFPT) method[25], respectively. The first Brillouin zone (BZ) is sampled by a $21\times 21\times 1$ k-point grid for electronic structures and C_{ij} , and $12\times 21\times 1$ for FM/antiferromagnetic (AFM) energies and e_{ij} .

MAIN CALCULATED RESULTS

For Janus CrS_{Cl} monolayer, as shown in Figure 1, Cr atoms are surrounded by six anions (three S and three Cl) to form a distorted octahedral structure, which exhibits a hexagonal lattice by Cl-Cr-S misalignment stacking with a space group of $P3m1$ (No.156). The difference in atomic size and electronegativity of S and Cl atoms will result in inequivalent Cr-S and Cr-Cl bonding lengths and charge distributions, which gives rise to intrinsic polar electric field and out-of-plane piezoelectric response. To confirm the magnetic ground state of CrS_{Cl}, we calculate the total energies of the FM and AFM configurations (see Figure 1). Calculated results show that the energy difference between AFM and FM orderings is 183 meV/rectangle supercell. So, the FM configuration is the ground state, which is related to the superexchange interaction. The optimized lattice constant a is 3.474 \AA , and the Cr-Cl-Cr and Cr-S-Cr bonding angles are 87.85° and 94.56° . Based on the Goodenough-Kanamori-Anderson (GKA) rules, FM superexchange interaction with near 90° will dominate the interaction between Cr atoms, which gives rise to the FM coupling[26, 27].

To verify the dynamical stability of CrS_{Cl}, we calculate its phonon spectra, as shown in Figure 2 (a). No negative frequency phonons are observed in the whole BZ, which implies that CrS_{Cl} is dynamically stable. To further confirm its thermal stability, we perform ab-initio molecular dynamics (AIMD) simulations at 300 K for 7 ps using a $4\times 4\times 1$ supercell and a time step of 1 fs. As shown in FIG.1 of electronic supplementary information

(ESI), during the simulation period, little energy fluctuation is observed and the structures at the end of the AIMD simulations show no structural transitions, indicating that CrS_{Cl} is stable at a temperature of 300 K. To determine the mechanical stability of CrS_{Cl}, the linear elastic constants are calculated, and the 2D elastic tensor (Voigt notation) with space group *P3m1* can be reduced into:

$$C = \begin{pmatrix} C_{11} & C_{12} & 0 \\ C_{12} & C_{11} & 0 \\ 0 & 0 & (C_{11} - C_{12})/2 \end{pmatrix} \quad (1)$$

Only two independent elastic constants ($C_{11}=62.82 \text{ Nm}^{-1}$ and $C_{12}=13.67 \text{ Nm}^{-1}$) can be observed, which meet Born-Huang criteria of mechanical stability ($C_{11} > 0$ and $C_{11} - C_{12} > 0$)^[28], thereby verifying mechanical stability of CrS_{Cl}.

For 2D hexagonal symmetric system with a typical triangle lattice structure, the magnetocrystalline direction determines type of magnetic phase transition. The in-plane one (an easy magnetization plane) means that there is no energetic barrier to the rotation of magnetization in the *xy* plane, which will produce a Berezinskii-Kosterlitz-Thouless magnetic transition to a quasi-long-range phase^[29, 30]. However, the out-of-plane one can give rise to a long-range FM phase. It is difficult to simulate quasi-long-range phase with in-plane magnetic anisotropy by DFT calculations. In previous studies, the electronic structures are calculated by assuming magnetocrystalline direction along *x* axis, which should be different from ones of quasi-long-range phase. For most 2D systems, the magnetocrystalline direction has small effects on their electronic properties. However, some essential influences on electronic and topological properties have been observed in some 2D materials^[31, 32]. Although the magnetocrystalline direction of 2D materials can be regulated by external magnetic field, the needed magnetic field may be very large (For example, the energetic barrier of 1 meV is equivalent to applying an external magnetic field of around 5-10 T.). Thus, it is very realistic to search for 2D out-of-plane magnetic materials with a typical triangle lattice structure. The intrinsic magnetic anisotropy of CrS_{Cl} can be determined by MAE. We define MAE as energy difference ($E_x - E_z$), where E_x/E_z is the energy per primitive cell when the magnetization is along the *x/z* direction. The positive/negative MAE means out-of-plane/in-plane direction. The calculated MAE is 36 μeV , indicating that the intrinsic easy axis of CrS_{Cl} is out-of-plane. Thus, CrS_{Cl} is a 2D long-range FM material.

The spin-resolved electronic band structures calculated by using GGA and GGA+SOC are plotted in Figure 2 (b) and (c). Around the Fermi level, the fully spin-polarized valence band and conduction band are in the same spin channels. The GGA results show that CrS_{Cl} is an indirect gap semiconductor (gap value of 1.98 eV) with both

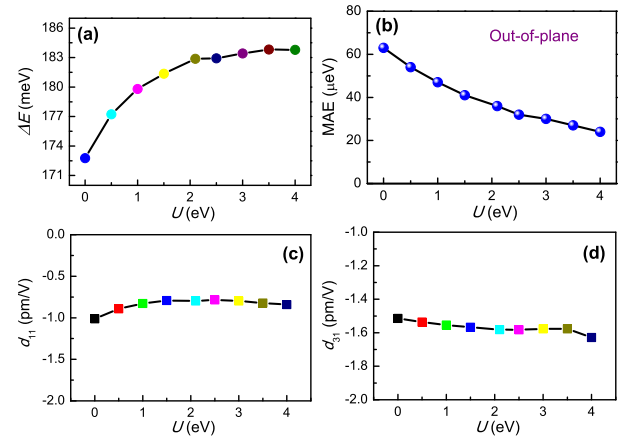


FIG. 3. (Color online) For CrS_{Cl} monolayer, the energy differences ΔE between AFM and FM ordering (a), MAE (b), d_{11} (c) and d_{31} (d) as a function of U .

the valence band maximum (VBM) and conduction band minimum (CBM) lying between the K and Γ points. It is noted that the two extrema of top valence band are very close, and the energy difference is only 5.3 meV. With the inclusion of SOC, the gap is reduced to 1.87 eV. Moreover, sizable Zeeman-type valley splitting occurs at the Γ point for spin-down direction, and the splitting is 66.5 meV. According to the Cr-*d* band structure projection (FIG.2 of ESI), the Cr atoms change from $4s^13d^5$ to $4s^03d^3$ in the electronic arrangement during the synthesis of CrS_{Cl}, which means that CrS_{Cl} would have a theoretical magnetic moment of 3 μ_B . Calculated results show a net magnetic moment of 3 μ_B per CrS_{Cl} chemical formula.

To simply estimate Curie temperature T_C , the spin Hamiltonian under the Heisenberg model can be expressed as:

$$H = -J \sum_{i,j} S_i \cdot S_j - A \sum_i (S_i^z)^2 \quad (2)$$

where J , S and A are the nearest exchange parameter, spin quantum number and MAE, respectively. By comparing energies of AFM (E_{AFM}) and FM (E_{FM}) configurations of CrCl₃Br with rectangle supercell, the J with normalized spin vector ($|S|=1$) is determined from these equations:

$$E_{AFM} = E_0 + 2J - 2A \quad E_{FM} = E_0 - 6J - 2A \quad (3)$$

$$J = \frac{E_{AFM} - E_{FM}}{8} \quad (4)$$

where E_0 is the energy without magnetic coupling. The normalized magnetic moment and auto-correlation as a function of temperature with $J=22.86$ meV are plotted in Figure 2 (d), and the predicted T_C is about 275 K.

TABLE I. For monolayer CrYX (Y=S and O; X=F, Cl, Br or I), the lattice constants a_0 (Å), the energy difference between AFM and FM ordering ΔE (meV), the magnetic anisotropy energy MAE (μ eV), the elastic constants C_{ij} (Nm $^{-1}$), the piezoelectric coefficients e_{ij} (10^{-10} C/m) and d_{ij} (pm/V).

Name	a_0	ΔE	MAE	C_{11}	C_{12}	e_{11}	e_{31}	d_{11}	d_{31}
CrSCl	3.474	183	36	62.82	13.67	-0.39	-1.21	-0.80	-1.58
CrSBr	3.560	189	52	61.19	13.27	-0.19	-0.71	-0.40	-0.96
CrSI	3.712	168	185	59.98	12.72	0.13	-0.02	0.28	-0.03
CrOF	3.039	80	150	113.98	25.19	-0.21	-0.97	-0.24	-0.70
CrOCl	3.175	33	136	102.67	25.14	1.05	0.22	1.35	0.18
CrOBr	3.259	5	120	102.13	26.51	1.59	0.79	2.10	0.61

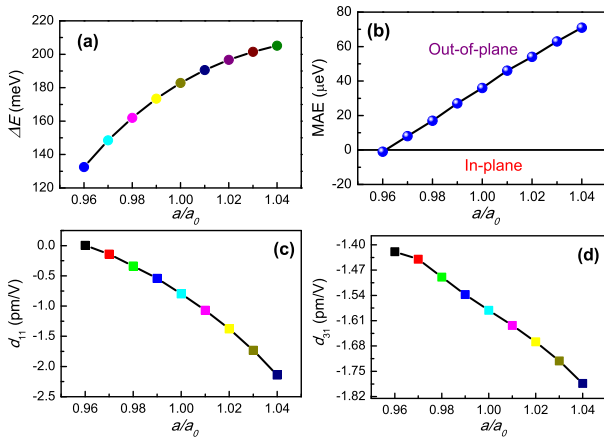


FIG. 4. (Color online) For CrSCl monolayer, the energy differences ΔE between AFM and FM ordering (a), MAE (b), d_{11} (c) and d_{31} (d) as a function of a/a_0 at $U=2.10$ eV.

Due to unique Janus structure of CrSCl, both in-plane and out-of-plane piezoelectric response can be observed. By using Voigt notation, the 2D piezoelectric stress and strain tensors for $P3m1$ symmetry can be reduced into[33, 34]:

$$e = \begin{pmatrix} e_{11} & -e_{11} & 0 \\ 0 & 0 & -e_{11} \\ e_{31} & e_{31} & 0 \end{pmatrix} \quad (5)$$

$$d = \begin{pmatrix} d_{11} & -d_{11} & 0 \\ 0 & 0 & -2d_{11} \\ d_{31} & d_{31} & 0 \end{pmatrix} \quad (6)$$

When an uniaxial in-plane strain is imposed, both in-plane and out-of-plane piezoelectric response can be induced ($e_{11}/d_{11} \neq 0$ and $e_{31}/d_{31} \neq 0$). However, by applying a biaxial in-plane strain, only out-of-plane piezoelectric response can exist ($e_{11}/d_{11}=0$, but $e_{31}/d_{31} \neq 0$). These mean that pure out-of-plane piezoelectric response can be achieved by imposed biaxial strain. Here, the two

independent d_{11} and d_{31} can be derived by $e_{ik} = d_{ij}C_{jk}$:

$$d_{11} = \frac{e_{11}}{C_{11} - C_{12}} \quad \text{and} \quad d_{31} = \frac{e_{31}}{C_{11} + C_{12}} \quad (7)$$

We use the orthorhombic supercell (see Figure 1) to calculate the e_{11}/e_{31} of CrClS. The calculated e_{11}/e_{31} is $-0.39 \times 10^{-10} / -1.21 \times 10^{-10}$ C/m with ionic part $0.29 \times 10^{-10} / 0.18 \times 10^{-10}$ C/m and electronic part $-0.68 \times 10^{-10} / -1.39 \times 10^{-10}$ C/m. For both e_{11} and e_{31} , the electronic and ionic contributions have opposite signs, and the electronic part dominates the piezoelectricity. And then, the d_{11}/d_{31} of CrSCl can be obtained from Equation 7, and the corresponding value is $-0.80 / -1.58$ pm/V. For most 2D materials, their out-of-plane piezoelectric response is less than 1 pm/V, such as oxygen functionalized MXenes (0.40-0.78 pm/V)[35], Janus TMD monolayers (0.03 pm/V)[33], functionalized h-BN (0.13 pm/V)[36], kalium decorated graphene (0.3 pm/V)[37], Janus group-III materials (0.46 pm/V)[38], Janus BiTeI/SbTeI monolayer (0.37-0.66 pm/V)[39], α -In₂Se₃ (0.415 pm/V)[40] and MoSO (0.7 pm/V)[41]. For the needs of practical application, a large out-of-plane piezoelectric response is highly desired to be compatible with the nowadays bottom/top gate technologies. Some progresses have been made for large out-of-plane piezoelectric response, such as NiClII (1.89 pm/V)[10], TePtS/TePtSe (2.4-2.9 pm/V)[42] and CrBr_{1.5}I_{1.5} (1.138 pm/V)[8]. However, compared with these materials, the CrSCl possesses out-of-plane FM ordering with high Curie temperature, which is beneficial to practical application. So, CrSCl is a potential PFM with large out-of-plane piezoelectric response.

To confirm reliability of large d_{31} , electronic correlation is considered to investigate piezoelectric properties of CrSCl. The lattice constants a at different U (0-4 eV) are optimized, and the change is about 0.066 Å with increasing U . It is found that CrSCl is always a FM ground state (see Figure 3 (a)), and the J changes from 21.60 meV to 22.97 meV with increasing U (variation of 1.37 meV), indicating that high T_C is robust against U . Moreover, the CrSCl has a steady out-of-plane magnetic anisotropy with increasing U (see Figure 3 (b)),

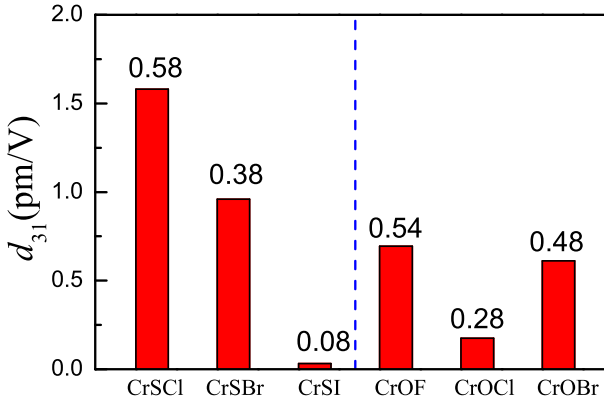


FIG. 5. (Color online) For monolayer CrYX (Y=S and O; X=F, Cl, Br or I), the piezoelectric strain coefficients d_{31} , and the electronegativity difference of X and Y atoms is given in the bar chart.

and the MAE decreases. The evolutions of energy band structures as a function of U are calculated by using GGA+SOC, and the gap versus U is plotted in FIG.3 of ESI. The CrSCl is always a semiconductor in considered U range, and the gap increases with increasing U . The elastic constants (C_{11} , C_{12} , $C_{11}-C_{12}$ and $C_{11}+C_{12}$) and piezoelectric stress coefficients (e_{11} and e_{31}) along the ionic and electronic contributions as a function of U are plotted in FIG.4 and FIG.5 of ESI. It is found that these elastic constants ($C_{11}-C_{12}$ and $C_{11}+C_{12}$) and piezoelectric stress coefficients (e_{11} and e_{31}) have weak dependence on U . The piezoelectric strain coefficients (d_{11} and d_{31}) versus U are plotted in Figure 3 (c) and (d). It is observed that the d_{31} (absolute value) is always larger than 1.51 pm/V within considered U range. Thus, the large d_{31} is robust against electronic correlation for CrSCl monolayer.

It is well known that the GGA may overestimate lattice constants of materials, and strain exists naturally in the process of synthesizing materials. So, the strain effects on piezoelectric properties of CrSCl are considered to confirm large d_{31} . The a/a_0 (0.96-1.04) is used to simulate biaxial strain, where a/a_0 denotes strained/unstrained lattice constant. Taking $U=2.1$ eV, we investigate the strain effects on physical properties of CrSCl. According to Figure 4 (a), all strained CrSCl are FM ground state in considered strain range. The tensile strain can enhance FM interaction, which makes for high Curie temperature. The normalized magnetic moment and auto-correlation as a function of temperature at $a/a_0=1.04$ are plotted in FIG.6 of ESI, and the predicted T_C is improved to 303 K. Figure 4 (b) shows that tensile strain can enhance MAE, while compressive strain can reduce MAE. At about $a/a_0=0.96$, the easy axis of CrSCl changes from out-of-plane to in-plane. In considered strain range, CrSCl maintains semiconductor characteristics, and the gap as a function of a/a_0 is plotted in FIG.7 of ESI. It

is found that the gap of CrSCl decreases with a/a_0 from 0.96 to 1.04. The elastic constants (C_{11} , C_{12} , $C_{11}-C_{12}$ and $C_{11}+C_{12}$) and piezoelectric stress coefficients (e_{11} and e_{31}) along the ionic and electronic contributions as a function of a/a_0 are plotted in FIG.8 and FIG.9 of ESI. The d_{11}/d_{31} versus a/a_0 is plotted in Figure 3 (c)/(d). It is found that increasing strain can improve d_{11} (absolute value) due to decreased $C_{11}-C_{12}$ and enhanced e_{11} (absolute). The d_{31} (absolute value) is also enhanced with increasing strain, which is due to reduced $C_{11}+C_{12}$. In considered strain range, the d_{31} (absolute value) is larger than 1.40 pm/V, indicating its robustness against strain. Calculated results show that tensile strain is beneficial to high Curie temperature, large MAE and large d_{11}/d_{31} (absolute value).

CONCLUSION

In fact, Janus monolayer CrSX (X=Cl, Br I) and CrOX (X=F, Cl, Br) have all been predicted to be out-of-plane FM semiconductors[15, 43], and we investigate their piezoelectric properties. The optimized lattice constants, energy difference between AFM and FM ordering, MAE, elastic constants and piezoelectric coefficients e_{ij}/d_{ij} are summarized in Table I. They all are mechanically stable due to satisfying criteria of mechanical stability for calculated elastic constants. The piezoelectric stress coefficients (e_{11} and e_{31}) along the ionic/electronic contribution are plotted in FIG.10 of ESI. It is found that, for both e_{11} and e_{31} , the electronic and ionic contributions have opposite signs. The d_{31} of CrSCl is the largest among CrSX (X=Cl, Br I), while the highest d_{31} among CrOX (X=F, Cl, Br) is CrOF, which may be explained by different atomic electronegativities of upper and lower layers. The d_{31} (absolute value) of CrYX (Y=S; X=Cl, Br I) and CrYX (Y=O; X=F, Cl, Br) along with the electronegativity difference of X and Y atoms are plotted in Figure 5. It is observed that the large electronegativity difference of X and Y atoms is related with large d_{31} . For CrSX (X=Cl, Br I), the d_{31} decreases with X from Cl to Br to I, and the d_{31} (absolute value) is only 0.03 pm/V due to very small electronegativity difference of S and I atoms. For CrOX (X=F, Cl, Br), the d_{31} decreases, and then increases, when X changes from F to Cl to Br.

In conclusion, the electronic structures, magnetic and piezoelectric properties of CrSCl are systematically investigated by first-principles calculations. Calculated results show that CrSCl is an out-of-plane FM semiconductor with high Curie temperature. Most importantly, the findings reveal that CrSCl exhibits large out-of-plane piezoelectric coefficient $|d_{31}|$ (>1.50 pm/V), which is very larger than those of most known 2D materials. It is found that out-of-plane FM ground state and large out-of-plane piezoelectric response are robust against

electronic correlation. The tensile strain can enhance FM interaction, MAE and $|d_{31}|$, which provide the alternative solution for enhancing out-of-plane piezoelectric effect. These comparisons about d_{31} (absolute value) of CrYX (Y=S; X=Cl, Br I) and CrYX (Y=O; X=F, Cl, Br) provide a development guide for searching Janus 2D materials with large out-of-plane piezoelectric response.

SUPPLEMENTARY MATERIAL

See the supplementary material for AIMD results; elastic and piezoelectric properties of CrSCl as a function of U or a/a_0 ; e_{ij} of CrYX (Y=S; X=Cl, Br I) and CrYX (Y=O; X=F, Cl, Br).

Conflicts of interest

There are no conflicts to declare.

This work was supported by Natural Science Basis Research Plan in Shaanxi Province of China (No. 2021JM-456). We are grateful to Shanxi Supercomputing Center of China, and the calculations were performed on TianHe-2.

[1] P. Lin, C. Pan and Z. L. Wang, Mater. Today Nano **4**, 17 (2018).

[2] S. D. Guo, W. Q. Mu, X. B. Xiao and B. G. Liu, Nanoscale **13**, 12956 (2021).

[3] Y. F. Zhao, Y. H. Shen, H. Hu, W. Y. Tong and C. G. Duan, Phys. Rev. B **103**, 115124 (2021).

[4] S. D. Guo, J. X. Zhu, W. Q. Mu and B. G. Liu, Phys. Rev. B **104**, 224428 (2021).

[5] J. H. Yang, A. P. Wang, S. Z. Zhang, J. Liu, Z. C. Zhong and L. Chen, Phys. Chem. Chem. Phys., **21**, 132 (2019).

[6] S. D. Guo, W. Q. Mu, Y. T. Zhu and X. Q. Chen, Phys. Chem. Chem. Phys. **22**, 28359 (2020).

[7] G. Song, C. F. Zhang, Z. Z. Zhang, G. N. Li, Z. W. Li, J. Du, B. W. Zhang, X. K. Huang and B. L. Gao, Phys. Chem. Chem. Phys. **24**, 1091 (2022).

[8] S. D. Guo, X. S. Guo, X. X. Cai, W. Q. Mu and W. C. Ren, J. Appl. Phys. **129**, 214301 (2021).

[9] G. Song, D. S. Li, H. F. Zhou et al., Appl. Phys. Lett. **118**, 123102 (2021).

[10] S. D. Guo, Y. T. Zhu, K. Qin and Y. S. Ang, Appl. Phys. Lett. **120**, 232403 (2022).

[11] M. Yagmurcukardes, Y. Qin, S. Ozen, M. Sayyad, F. M. Peeters, S. Tongay and H. Sahin, Appl. Phys. Rev. **7**, 011311 (2020).

[12] L. Zhang, Z. J. F. Yang, T. Gong et al., J. Mater. Chem. A **8**, 8813 (2020).

[13] A.-Y. Lu, H. Zhu, J. Xiao, C.-P. Chuu, Y. Han, M.-H. Chiu, C.-C. Cheng, C.-W. Yang, K.-H. Wei, Y. Yang, Y. Wang, D. Sokaras, D. Nordlund, P. Yang, D. A. Muller, M.-Y. Chou, X. Zhang and L.-J. Li, Nat. Nanotechnol. **12**, 744 (2017).

[14] J. Zhang, S. Jia, I. Kholmanov, L. Dong, D. Er, W. Chen, H. Guo, Z. Jin, V. B. Shenoy, L. Shi and J. Lou, ACS Nano **11**, 8192 (2017).

[15] Y. S. Hou, F. Xue, L. Qiu, Z. Wang and R. Q. Wu, npj Comput. Mater. **8**, 120 (2022).

[16] S. D. Guo, W. Q. Mu, H. T. Guo, Y. L. Tao and B. G. Liu, arXiv:2206.02081 (2022).

[17] P. Hohenberg and W. Kohn, Phys. Rev. **136**, B864 (1964); W. Kohn and L. J. Sham, Phys. Rev. **140**, A1133 (1965).

[18] G. Kresse, J. Non-Cryst. Solids **193**, 222 (1995).

[19] G. Kresse and J. Furthmüller, Comput. Mater. Sci. **6**, 15 (1996).

[20] G. Kresse and D. Joubert, Phys. Rev. B **59**, 1758 (1999).

[21] J. P. Perdew, K. Burke and M. Ernzerhof, Phys. Rev. Lett. **77**, 3865 (1996).

[22] S. L. Dudarev, G. A. Botton, S. Y. Savrasov, C. J. Humphreys and A. P. Sutton, Phys. Rev. B **57**, 1505 (1998).

[23] A. Togo, F. Oba, and I. Tanaka, Phys. Rev. B **78**, 134106 (2008).

[24] L. Liu, X. Ren, J. H. Xie, B. Cheng, W. K. Liu, T. Y. An, H. W. Qin and J. F. Hu, Appl. Surf. Sci. **480**, 300 (2019).

[25] X. Wu, D. Vanderbilt and D. R. Hamann, Phys. Rev. B **72**, 035105 (2005).

[26] J. B. Goodenough, Phys. Rev. **100**, 564 (1955).

[27] J. Kanamori, J. Phys. Chem. Solid **10**, 87 (1959).

[28] R. C. Andrew, R. E. Mapasha, A. M. Ukpong and N. Chetty, Phys. Rev. B **85**, 125428 (2012).

[29] K. Sheng, Q. Chen, H. K. Yuan and Z. Y. Wang, Phys. Rev. B **105**, 075304 (2022).

[30] S. Zhang, R. Xu, W. Duan, and X. Zou, Adv. Funct. Mater. **29**, 1808380 (2019).

[31] S. Li, Q. Q. Wang, C. M. Zhang, P. Guo and S. A. Yang, Phys. Rev. B **104**, 085149 (2021).

[32] H. Sun, S. S. Li, W. X. Ji and C. W. Zhang, Phys. Rev. B **105**, 195112 (2022).

[33] L. Dong, J. Lou and V. B. Shenoy, ACS Nano, **11**, 8242 (2017).

[34] M. N. Blonsky, H. L. Zhuang, A. K. Singh and R. G. Hennig, ACS Nano **9**, 9885 (2015).

[35] J. Tan, Y. H. Wang, Z. T. Wang, X. J. He, Y. L. Liu, B. Wang, M. I. Katsnelson and S. J. Yuan, Nano Energy **65**, 104058 (2019).

[36] A. A. M. Noor, H. J. Kim and Y. H. Shin, Phys. Chem. Chem. Phys. **16**, 6575 (2014).

[37] M. T. Ong and E. J. Reed, ACS Nano **6**, 1387 (2012).

[38] Y. Guo, S. Zhou, Y. Z. Bai, and J. J. Zhao, Appl. Phys. Lett. **110**, 163102 (2017).

[39] S. D. Guo, X. S. Guo, Z. Y. Liu and Y. N. Quan, J. Appl. Phys. **127**, 064302 (2020).

[40] L. Hu and X. R. Huang, RSC Adv. **7**, 55034 (2017).

[41] M. Yagmurcukardes and F. M. Peeters, Phys. Rev. B **101**, 155205 (2020).

[42] Z. Kahraman, A. Kandemir, M. Yagmurcukardes and H. Sahin, J. Phys. Chem. C **123**, 4549 (2019).

[43] R. J. Sun, R. Liu, J. J. Lu, X. W. Zhao, G. C. Hu, X. B. Yuan and J. F. Ren, Phys. Rev. B **105**, 235416 (2022).